Observation of dynamical vortices after quenches in a system with topology

N. Fläschner, D. Vogel, M. Tarnowski, B. S. Rem, D.-S. Lühmann, Markus Heyl, J. C. Budich, L. Mathey, K. Sengstock, C. Weitenberg

Observation of dynamical vortices after quenches in a system with topology

N. Fläschner[1,2], D. Vogel[1], M. Tarnowski[1,2], B. S. Rem[1,2], D.-S. Lühmann[1], M. Heyl[3], J. C. Budich[4,5], L. Mathey[1,2,6], K. Sengstock [iD][1,6]* and C. Weitenberg [iD][1,2]

Topological phases constitute an exotic form of matter characterized by non-local properties rather than local order parameters[1]. The paradigmatic Haldane model on a hexagonal lattice features such topological phases distinguished by an integer topological invariant known as the first Chern number[2]. Recently, the identification of non-equilibrium signatures of topology in the dynamics of such systems has attracted particular attention[3–6]. Here, we experimentally study the dynamical evolution of the wavefunction using time- and momentum-resolved full state tomography for spin-polarized fermionic atoms in driven optical lattices[7]. We observe the appearance, movement and annihilation of dynamical vortices in momentum space after sudden quenches close to the topological phase transition. These dynamical vortices can be interpreted as dynamical Fisher zeros of the Loschmidt amplitude[8], which signal a so-called dynamical phase transition[9,10]. Our results pave the way to a deeper understanding of the connection between topological phases and non-equilibrium dynamics.

The discovery of topological matter has revolutionized our understanding of band theory: not only are the dispersions of the energy bands important, but so is the geometry of the corresponding eigenstates[1]. The non-local nature of the topological invariants characterizing such phases goes beyond the Landau paradigm of local order parameters and leads to topological protection, for example, against disorder. Ultracold quantum gases in optical lattices allow for controlled studies of archetypal topological models[11–14]. In addition, compared with, for example condensed-matter systems, they also allow for detailed studies of the relation between dynamics and topology as the timescales are experimentally easier to access. Dynamical studies of driven systems have recently attracted attention in terms of their high T_c superconductivity[15]. A particular challenge is to identify non-equilibrium signatures of topology in the dynamics of highly excited states[3,4,16]. Here, we observe the time evolution of the wavefunction after a sudden quench in a Haldane-like model and find dynamical vortices as a signature of the topological nature of the underlying ground state.

In the experiments described here, the state tomography method allows mapping of the full quantum-mechanical wavefunction of non-interacting ultracold fermionic quantum gases in an optical lattice for any time after a sudden quench of the system close to or into a Chern insulating phase. As a key result, we identify in an intense series of measurements the appearance, movement and annihilation
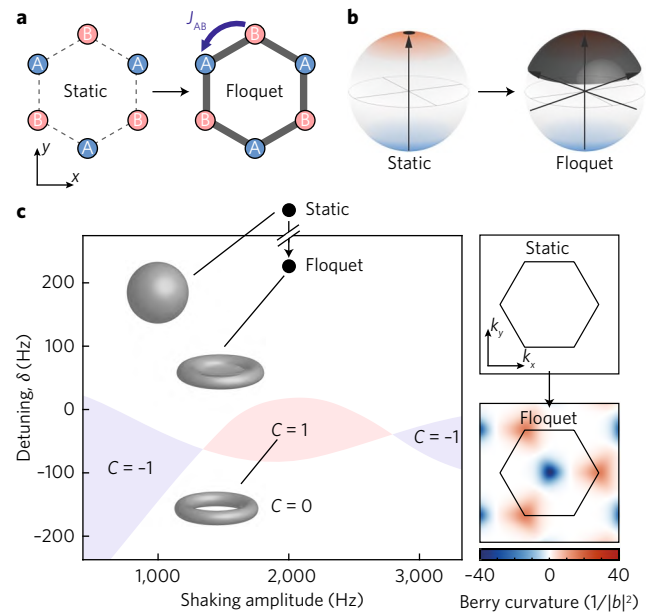

Fig. 1 | Quenches in the topological Haldane model. a, We realized a quench between two Hamiltonians on a hexagonal lattice. In the initial system, tunnelling J_{AB} between the A and B sites is suppressed by a large energy offset. In the final Floquet system, tunnelling is re-established by means of near-resonant driving. **b**, At each momentum, the Hamiltonian describes the coupling between the states of the A and B sublattices, and can be visualized on a Bloch sphere. In the initial system, the Hamiltonian for all momenta points to the north pole, whereas in the Floquet system, the Hamiltonian covers a large surface of the Bloch sphere. **c**, Phase diagram for the Floquet Hamiltonian as a function of shaking amplitude and detuning with respect to the sublattice offset for the case of circular lattice shaking. The model is Haldane-like with topological phase transitions to regions with Chern number, C, 1 and −1. We suddenly jump from effectively infinite detuning to a point in the vicinity of a topological phase transition, which has pronounced Berry curvature (insets). The Berry curvature is given in units set by the length $|b|$ of the reciprocal lattice vectors. The grey schematics show the strong change of curvature in the vicinity of the topological phase transition even before the appearance of a hole. The Floquet phase diagram is calculated for a shaking frequency of 11.236 kHz and a variable sublattice offset (see Supplementary Information).

[1]ILP - Institut für Laserphysik, Universität Hamburg, Hamburg, Germany. [2]The Hamburg Centre for Ultrafast Imaging, Hamburg, Germany. [3]Physik Department, Technische Universität München, Garching, Germany. [4]Institute for Quantum Optics and Quantum Information of the Austrian Academy of Sciences, Innsbruck, Austria. [5]Institute for Theoretical Physics, University of Innsbruck, Innsbruck, Austria. [6]ZOQ - Zentrum für Optische Quantentechnologien, Universität Hamburg, Hamburg, Germany. N. Fläschner, D. Vogel and M. Tarnowski contributed equally to this work. *e-mail: klaus.sengstock@physnet.uni-hamburg.de
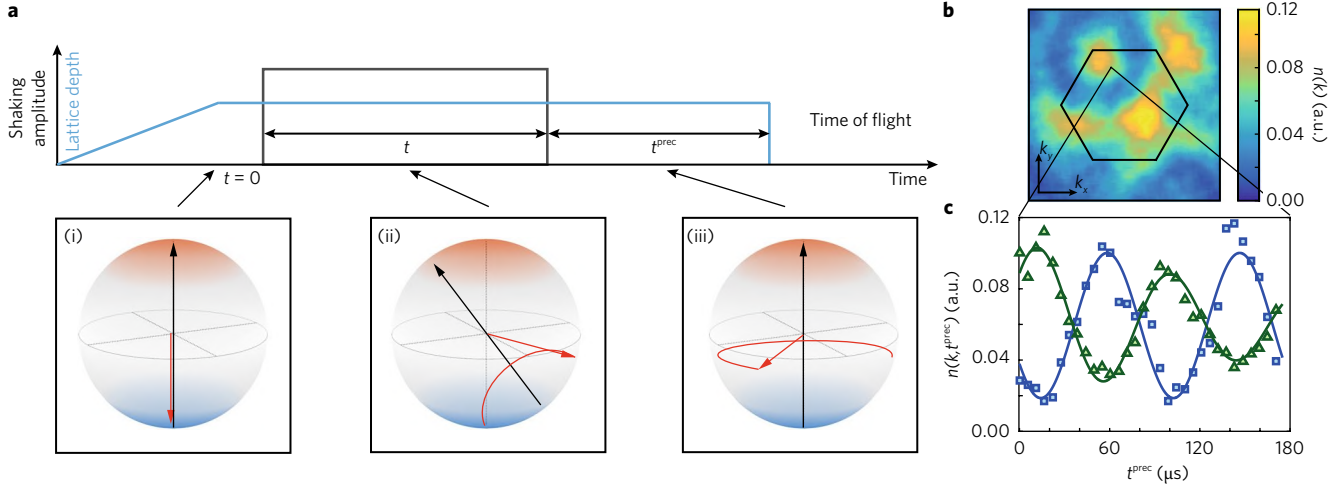
Fig. 2 | Experimental sequence for time-resolved state tomography. a, With an adiabatic ramp up of the lattice depth, we prepare all momentum states (red arrow) in the lower eigenstate of the static Hamiltonian (black arrow), that is, pointing to the south pole (i). We quench into the Floquet Hamiltonian by suddenly switching on the driving amplitude, which leads to the dynamics of the state according to the new Hamiltonian for a time t (ii). To measure the evolved state, we quench back into the initial Hamiltonian, such that the state precesses around the vertical axis for a time t^{prec} (iii). **b**, We measure the momentum density $n(k)$ via time-of-flight expansion. The picture shows an example at $t = 0.543$ ms and $t^{prec} = 93.5$ μs and for the parameters given in Fig. 3. **c**, The precession leads to an oscillation in the momentum density $n(k, t^{prec}) \sim [1 + A_k \sin(\omega_k t^{prec} + \varphi_{k,t})]$ (compare ref. [7]), the phase of which is the azimuthal phase $\varphi_{k,t}$ of the state at the end of the dynamics in the Floquet system. We evaluate this oscillation at each pixel of our images, that is, each momentum, and for each evolution time t (blue and green data points show the oscillation at the indicated pixel for the evolution times $t = 0.267$ ms and 0.801 ms, respectively).

of vortex pairs in the momentum state of the many-body fermionic wavefunction. Fascinatingly, these vortices that appear dynamically after the quench are the same topological defects that also characterize the ground state of our system in the form of Dirac points. This relation demonstrates the interesting new connection between topological structures in highly excited states that are dynamically reached and the underlying ground-state topology.

In the following, we describe in detail the experimental studies. The initial state is a fermionic band insulator in the lowest band of a hexagonal lattice[17] with a large offset between the A and B sites such that tunnelling is suppressed (Fig. 1a). The final Hamiltonian after the quench is realized as a Floquet Hamiltonian and is engineered by means of resonant circular lattice shaking[7,11,18,19] and re-establishes tunnelling. The initial Hamiltonian features flat bands with vanishing Berry curvature, while the final Hamiltonian realizes a Haldane-like model with tunable Berry curvature[2,11]. Due to the fermionic statistics, the many-body state of the spin-polarized fermions is given by the Slater determinant of single momentum modes. In a two-band model, the Hamiltonian and the time-evolved modes can be visualized on a Bloch sphere for each quasi-momentum (Fig. 1b). If we choose the poles of the Bloch sphere as the eigenmodes of the initial Hamiltonian, the initial modes of the lowest band point to the south pole. The azimuthal phase $\varphi_{k,t}$ and polar angle $\theta_{k,t}$ on the Bloch sphere then describe the momentum modes after the time evolution. For our parameters, the final Hamiltonian points to different directions for each quasi-momentum (Fig. 1b), leading to pronounced Berry curvature. The circular shaking breaks time-reversal symmetry, such that the final Haldane-like Hamiltonian can also have bands with non-trivial Chern numbers[11] (Fig. 1c). Here, we move to a parameter regime with strong Berry curvature in the vicinity of the topological phase transition.

Our experimental sequence starts with a lattice ramp to prepare fermions filling up the lowest band (Fig. 2a). The quench is realized by suddenly switching on the lattice driving, which induces dynamics according to the new Hamiltonian. To measure the dynamics of the many-body wavefunction, we employ time-resolved state tomography after various evolution times t (refs [7,20]). For the tomography,

we project back onto the eigenstates of the initial Hamiltonian and observe the ensuing momentum-dependent precession on the Bloch sphere, which translates into a density oscillation after a time-of-flight expansion (Fig. 2b). We observe this oscillation by taking a series of absorption images with a high momentum resolution of 2,800 pixels within the first Brillouin zone. By a pixel-wise evaluation of the phase of the oscillation (Fig. 2c), we obtain the momentum-resolved azimuthal phase profile $\varphi_{k,t}$ of the many-body state for each evolution time.

Characteristic data featuring the vortex dynamics are shown in Fig. 3. The many-body wave function, which starts with all momentum modes at the south pole, spreads on the Bloch sphere and reaches the north pole in the third time step (Fig. 3a). When plotting the momentum-resolved phase profile $\varphi_{k,t}$ of the same data (Fig. 3b), we see that reaching the north pole corresponds to the appearance of a vortex–anti-vortex pair in momentum space. These dynamical vortices move through momentum space and annihilate at a later time. In addition, we observe static vortices in the centre and at three equivalent corners of the first Brillouin zone, which remain for all evolution times. The static vortices can be identified with the south pole of the Bloch sphere, where no dynamics occurs, while the dynamical vortices correspond to the north pole, which is transiently reached for different momenta at different times[21]. When one momentum mode is at the north pole, the neighbouring momentum modes occupy a patch around the pole and therefore the corresponding azimuthal phases carry a winding.

The observed appearance of dynamical vortices can be translated into the language of a dynamical phase transition in the sense of ref. [9]. This concept exploits a formal analogy between the non-analytic behaviour of the free energy at equilibrium phase transitions and a similar non-analytic behaviour of dynamical quantities at critical times after quantum quenches[22]. It was introduced for quantum Ising models[9], extended to Hubbard models[23] and topological lattice Hamiltonians[24–26], and in parallel to this work also experimentally studied with trapped ions[27]. In analogy to the Fisher zeros (or Lee–Yang zeros) in the partition function, which trigger equilibrium
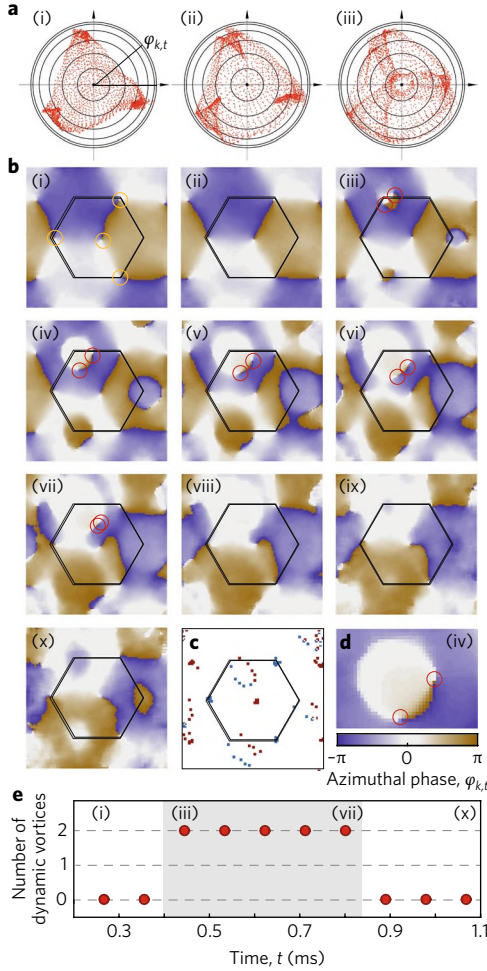
Fig. 3 | Observation of dynamical vortices in momentum space.
a, Visualization of the experimental data on the Bloch sphere viewed from the south pole for different stroboscopic evolution times (multiples of the Floquet driving period of 89 μs starting with 267 μs). **b**, Phase profiles $\varphi_{k,t}$ of the same data including additional time steps. The hexagon marks the first Brillouin zone. Static vortices (marked by orange circles in (i)) are imprinted from the final Hamiltonian[7] and remain fixed for all times. Additionally, dynamical vortices appear, move and disappear during the time evolution (marked by red circles). **c**, Position of the vortices summed over all observed evolution times (blue and red dots for clockwise and anticlockwise phase winding, respectively). The dynamical vortices are created and annihilated as vortex–anti-vortex pairs and they move on a closed contour in momentum space. **d**, Zoom-in of the phase profile at time step (iv) demonstrating our high momentum resolution. **e**, The number of dynamical vortices in the first Brillouin zone as a function of evolution time. The grey shaded area marks the time interval during which the dynamical vortices are present. The shaking amplitude is 2 kHz and the shaking detuning from the sublattice offset of 11.460 kHz is 220 Hz. For details on the lattice set-up see Methods.

phase transitions, one can define dynamical Fisher zeros[8], at which the Loschmidt amplitude $G(t) = \langle \psi_0 \mid \exp(-iHt/\hbar) \mid \psi_0 \rangle$ goes to zero. It measures the overlap of the time-evolved many-body state with the initial state $\mid \psi_0 \rangle$ before the quench. The overlap vanishes exactly if at least one of the momentum modes reaches the north pole, which establishes the connection to the appearance of vortices that we observe. Therefore, the observed dynamical vortices can be identified with these dynamical Fisher zeros and be regarded as a signature of a dynamical phase transition as in the sense of ref. [9]. Details on the connection to the dynamical phase transition and a plot of the calculated non-analytical behaviour can be found in
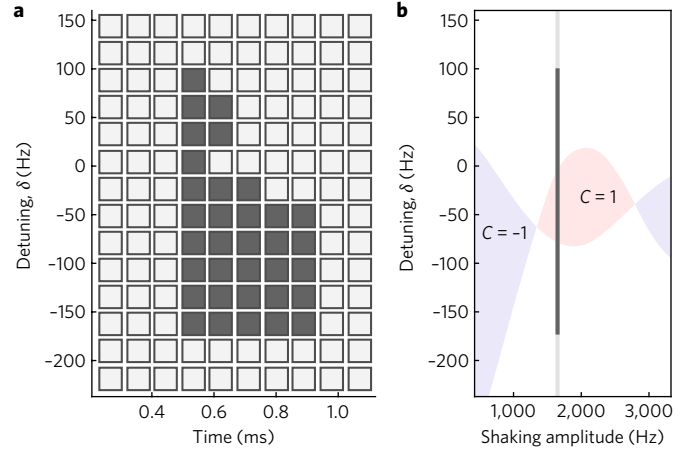

Fig. 4 | Relation between the occurrence of dynamical vortices and the equilibrium phase diagram. a, The presence of dynamical vortices as a function of evolution time t and detuning δ between the AB-offset and the shaking frequency. Dark (light) grey boxes refer to the presence (absence) of dynamical vortices. **b**, The topological phase diagram of the underlying final Floquet Hamiltonian as a function of detuning and shaking amplitude features non-trivial Chern numbers for suitable parameters. The vertical bar denotes the path of endpoints of the sudden quench that was traced out in the experiment (shaking amplitude 1.65 kHz) and the darker colour indicates the region where dynamical vortices were observed.

the Supplementary Information. We note, however, that the term dynamical phase transition is also used in different contexts, for example, in disordered systems as a transition between localized and non-localized states[28–30].

We repeated the experiment for different final Hamiltonians by shaking at different detunings (Fig. 4) and we observed the appearance of dynamical vortices for quenches into a region within and closely around the non-trivial regime of the final Hamiltonian. These observations raise the question whether the appearance of dynamical vortices is a signature for the change of Chern number between the initial and final Hamiltonian. Indeed, one can prove that a change of Chern number does imply the appearance of dynamical vortices[10]. However, a strong change in Berry curvature across the quench, as it appears close to the topological phase transition, is also sufficient to induce dynamical vortices (named accidental vortices[10]). Motivated by our studies on the relation between dynamics and topology, recently, two reports[21,31] showed a detailed relation between the so-called linking number and topology. For our system, that work also shows that the existence of dynamical vortices depends on both the initial and the final Hamiltonian and only when the initial Hamiltonian corresponds to infinitely flat bands does one expect a one-to-one relation[21,31].

Instead, the Chern number of the final Hamiltonian can be inferred from the contour in momentum space, which is traced out by the dynamical vortex pair. For a Chern number of plus or minus one, the contour is expected to enclose one of the static vortices, whereas for Chern number zero, it does not[31]. For the parameters of Fig. 3, where the quench is to a system with zero Chern number, the contour does not wind around the static vortices (Fig. 3c). In the measurements presented here, the rather flat bands for the tomography and correspondingly small parameter regime for the area with Chern number one, in combination with the averaging over the inhomogeneous system, prevented us from observing non-trivial contours. Very recently we could, however, experimentally realize the direct mapping between non-trivial contours with

corresponding linking number and non-trivial Chern numbers in a system with dispersive bands[32].

We have observed the appearance, movement and annihilation of dynamical vortices in momentum space in the far-from-equilibrium dynamics following a sudden quench of the system parameters. These dynamical vortices are deeply related to the underlying topological phase diagram and can be used to approximately locate the phase transitions. While it is often experimentally challenging to reach the ground state of relevant systems[5,6], the observation of such dynamics in highly excited states might be an alternative approach for the exploration of the underlying ground-state phase diagram, in cases where a thorough connection between equilibrium and dynamical phase transitions can be established[31]. This might open a promising route to study complex phase diagrams such as the Fermi–Hubbard model or interacting topological phases.

Methods

Methods, including statements of data availability and any associated accession codes and references, are available at https://doi.org/10.1038/s41567-017-0013-8.

References

1. Hasan, M. Z. & Kane, C. L. Colloquium: topological insulators. *Rev. Mod. Phys.* **82**, 3045–3067 (2010).
2. Haldane, F. D. M. Model for a Quantum Hall effect without Landau levels: condensed-matter realization of the "parity anomaly". *Phys. Rev. Lett.* **61**, 2015–2018 (1988).
3. Hu, Y., Zoller, P. & Budich, J. C. Dynamical buildup of a quantized Hall response from nontopological states. *Phys. Rev. Lett.* **117**, 126803 (2016).
4. Ünal, F. N., Mueller, E. J. & Oktel, Ö. Noneqilibrium fraction Hall response after a topological quench. *Phys. Rev. A* **94**, 053604 (2016).
5. Caio, D. M., Cooper, N. R. & Bhaseen, M. J. Quantum quenches in Chern insulators. *Phys. Rev. Lett.* **115**, 236403 (2015).
6. D'Alessio, L. & Rigol, M. Dynamical preparation of Floquet Chern insulators. *Nat. Commun* **6**, 8336 (2015).
7. Fläschner, N. et al. Experimental reconstruction of the Berry curvature in a Floquet Bloch band. *Science* **352**, 1091–1094 (2016).
8. Brandner, K., Maisi, V. F., Pekola, J. P., Garrahan, J. P. & Flindt, C. Experimental observation of dynamical Lee-Yang zeros. *Phys. Rev. Lett.* **118**, 180601 (2017).
9. Heyl, M., Polkovnikov, A. & Kehrein, S. Dynamical quantum phase transitions in the transverse-field Ising model. *Phys. Rev. Lett.* **110**, 135704 (2013).
10. Vajna, S. & Dora, B. Topological classification of dynamical phase transitions. *Phys. Rev. B* **91**, 155127 (2015).
11. Jotzu, G. et al. Experimental realization of the topological Haldane model with ultracold fermions. *Nature* **515**, 237–240 (2014).
12. Aidelsburger, M. et al. Measuring the Chern number of Hofstadter bands with ultracold bosonic atoms. *Nat. Phys* **11**, 162–166 (2015).
13. Kennedy, C. J., Burton, W. C., Chung, W. C. & Ketterle, W. Observation of Bose–Einstein condensation in a strong synthetic magnetic field. *Nat. Phys* **11**, 859–864 (2015).
14. Eckardt, A. Colloquium: atomic quantum gases in periodically driven optical lattices. *Rev. Mod. Phys.* **89**, 011004 (2017).
15. Fausti, D. et al. Light-induced superconductivity in a stripe-ordered cuprate. *Science* **331**, 189–191 (2011).
16. Polkovnikov, A., Sengupta, K., Silva, A. & Vengalattore, M. Colloquium: nonequilibrium dynamics of closed interacting quantum system. *Rev. Mod. Phys.* **83**, 863–883 (2011).
17. Soltan-Panahi, P. et al. Multi-component quantum gases in spin-dependent hexagonal lattices. *Nat. Phys* **7**, 434–440 (2011).
18. Parker, C. V., Ha, L.-C. & Chin, C. Direct observation of effective ferromagnetic domains of cold atoms in shaken optical lattices. *Nat. Phys* **9**, 769–774 (2013).
19. Zheng, W. & Zhai, H. Floquet topological states in shaking optical lattices. *Phys. Rev. A* **89**, 061603 (2014). (R).
20. Hauke, P., Lewenstein, M. & Eckardt, A. Tomography of band insulators from quench dynamics. *Phys. Rev. Lett.* **113**, 045303 (2014).
21. Yu, J. Phase vortices of the quenched Haldane model. *Phys. Rev. A* **96**, 023601 (2017).
22. Heyl, M. Scaling and universality at dynamical quantum phase transitions. *Phys. Rev. Lett.* **115**, 140602 (2015).
23. Canovi, E., Werner, P. & Eckstein, M. First-order dynamical phase transitions. *Phys. Rev. Lett.* **113**, 265702 (2014).
24. Schmitt, M. & Kehrein, S. Dynamical quantum phase transitions in the Kitaev honeycomb model. *Phys. Rev. B* **92**, 075114 (2015).
25. Budich, J. C. & Heyl, M. Dynamical topological order parameters far from equilibrium. *Phys. Rev. B* **93**, 085416 (2016).
26. Huang, Z. & Balatsky, A. V. Dynamical quantum phase transitions: role of topological nodes in wave function overlaps. *Phys. Rev. Lett.* **117**, 086802 (2016).
27. Jurcevic, P. et al. Direct observation of dynamical quantum phase transitions in an interacting many-body system. *Phys. Rev. Lett.* **119**, 080501 (2017).
28. Billy, J. et al. Anderson localization of a non-interacting Bose–Einstein condensate. *Nature* **453**, 891–894 (2008).
29. Roati, G. et al. Direct observation of Anderson localization of matter waves in a controlled disorder. *Nature* **453**, 895–898 (2008).
30. Schreiber, M. et al. Observation of many-body localization of interacting fermions in a quasirandom optical lattice. *Science* **349**, 842–845 (2015).
31. Wang, C., Zhang, P., Chen, X., Yu, J. & Zhai, H. Measuring topological number of a Chern-insulator from quench dynamics. *Phys. Rev. Lett.* **118**, 185701 (2017).
32. Tarnowski, M. et al. Characterizing topology by dynamics: chern number from linking number. Preprint at http://arXiv.org/abs/1709.01046 (2017).

Author contributions

N.F., D.V. and M.T. took and analysed the data and performed numerical simulations. C.W., B.S.R. and K.S. conceived the experiment. All authors contributed to the interpretation of the data and to the writing of the manuscript.

Competing interests

The authors declare no competing financial interests.

Additional information

Supplementary information is available for this paper at https://doi.org/10.1038/s41567-017-0013-8.

Reprints and permissions information is available at www.nature.com/reprints.

Correspondence and requests for materials should be addressed to K.S.

Publisher's note: Springer Nature remains neutral with regard to jurisdictional claims in published maps and institutional affiliations.

Methods

Optical lattice. We employed a hexagonal optical lattice with tunable energy offset Δ_{AB} between the A- and B-sublattice on-site energies. The lattice is formed by three running interfering laser beams. For more details on the lattice set-up, see ref. [7].

The two lowest bands of this lattice can be well described within a tight-binding model with the eigenbasis being the Bloch states restricted to the A- and B-sublattice sites. In this basis, the quasi-momentum-dependent Hamiltonian reads

$$\widehat{H}(\mathbf{k}) = \begin{pmatrix} \dfrac{\Delta_{AB}}{2} + \sum_i 2J_{AA}\cos(\mathbf{k}\cdot\mathbf{a}_i) & \sum_i J_{AB}\exp(-i\mathbf{k}\cdot\mathbf{d}_i) \\ \sum_i J_{AB}\exp(i\mathbf{k}\cdot\mathbf{d}_i) & -\dfrac{\Delta_{AB}}{2} + \sum_i 2J_{BB}\cos(\mathbf{k}\cdot\mathbf{a}_i) \end{pmatrix}$$

with the next-nearest-neighbour hopping amplitudes J_{AA} and J_{BB} on the diagonal and the nearest-neighbour hopping amplitude J_{AB} on the off-diagonal element, which couples the A and B sites.

The Bravais vectors connecting neighbouring A(B) sites with each other are, for our purely hexagonal lattice structure, $a_1 = -4\pi/(3k_L)(0\ 1\ 0)$, $a_2 = -4\pi/(3k_L)\left(\sqrt{3}/2\ 1/2\ 0\right)$, and $a_3 = a_2 - a_1$. The d_i connect A sites with neighbouring B sites $d_1 = 1/3(a_1 + a_2)$, $d_2 = 1/3(-2a_1 + a_2)$, and $d_3 = 1/3(a_1 - 2a_2)$. The lattice vector k_L is given by the wavelength of the laser forming the lattice $k_L = 2\pi/1,064$ nm.

All tight-binding parameters of the lattice can be expressed as a function of the single parameter Δ_{AB}, once the polarizations of the lattice beams, which determine the geometry[7], are fixed. The lattice polarizations are tilted out of the lattice plane by an angle of 9° and the out-of-plane polarization components of the three beams are phase shifted relative to the in-plane polarizations by 0, $2\pi/3$ and $4\pi/3$, respectively. We therefore use Δ_{AB} as a measure for the lattice depth throughout the manuscript. For our polarization setting and for the parameter regime of Δ_{AB} presented in the main text and here in the Methods, we determine the relations from a fit to exact band structure calculations:

$$J_{AB}/E_R \approx 0.221(\Delta_{AB}/E_R)^{-1.4}, \ J_{AA}/E_R \approx 0.0529(\Delta_{AB}/E_R)^{-2.05}, \ \text{and} \ J_{BB} \approx 0$$

Here, $E_R/h = 4,410$ Hz is the recoil frequency and h is Planck's constant. All data were taken in a configuration with large Δ_{AB}/h ranging from 10,750 Hz to 11,460 Hz, which leads to tunnelling amplitudes J_{AB}/h ranging from 280 Hz to 256 Hz, J_{AA}/h ranging from 38 Hz to 33 Hz and $J_{BB}/h \approx 0$, such that Δ_{AB} is the dominating energy scale and the initial bands are nearly flat.

Since the position of the lattice is determined by the relative phases of the three running laser beams forming the lattice, we can move the lattice in real space by frequency modulating the laser beams using acousto-optical modulators (AOMs). To realize circular lattice shaking as used for all experiments presented in the main text, two of the three AOMs are driven by computer programmable digital frequency sources with a time-dependent frequency $\nu_{1,2}(t) = 110$ MHz $+ 2A_s[\pm\cos(2\pi\,\nu_s t) + \sqrt{3}\sin(2\pi\,\nu_s t)]$, where A_s and ν_s are the shaking amplitude and frequency, respectively. The shaking frequency is $\nu_s = 11,236$ Hz for all data and the shaking amplitude is $A_s = 2$ kHz for the data shown in Fig. 3 and 1.65 kHz for the data shown in Fig. 4.

Data acquisition and analysis. Our experiments start with a spin-polarized $(F = 9/2, m_F = 9/2)$ cloud of 1×10^5 fermionic ^{40}K atoms in a non-interacting band insulator in the lowest band of the two-dimensional initial lattice. In the transverse direction, the potential is harmonic, thus forming a lattice of tubes. The external confinement from the shape of the lattice beams and additional dipole trap beams leads to trapping frequencies of $\nu_{x,y,z} = (83(4), 108(5), 93(4))$ Hz.

The full state tomography method is explained in the main text and in more detail in ref. [7]. To resolve the precession dynamics after the projection onto the eigenstates of the initial Hamiltonian, we take 32 images at varying times t^{prec} after this projection with a step size of 5.5 μs. In the data analysis, we apply a 5×5 pixel Gaussian filter of width of 5 pixel on the atomic density of each time step, but no temporal filtering. With a length of the reciprocal lattice vector of 58(2) pixels, we have more than 2,800 pixels in the first Brillouin zone and therefore a very high resolution in momentum space. For every pixel, we fit a damped oscillation to the density of the form

$$n(k, t^{prec}) = W_k\left[1 + \alpha_k\exp\left(-\gamma_k t^{prec}\right)\sin\left(2\pi\nu_0 t^{prec} + \varphi_k\right)\right]$$

with the envelope W_k, the oscillation amplitude α_k, the damping γ_k, the oscillation frequency ν_0 and the phase φ_k. To minimize the number of fit parameters, we fix

the frequency in the fit to $\nu_0 = 11.364$ kHz, which is the third Fourier component for these time steps. We initialize the phases by the values from a fast Fourier transform estimator and the amplitudes from the difference of the minimal and maximal values.

Relation between the occurrence of dynamical vortices and the equilibrium phase diagram. When repeating the quench experiments for different final Hamiltonians, we observe dynamical vortices both for parameters for which non-zero Chern numbers are expected but also within the close vicinity of this region (Fig. 4). While the region with non-zero Chern number has a width of approximately 80 Hz, we observe dynamical vortices for detunings centered around this region but with a broader range of 280 Hz width, which corresponds to the AB-tunnelling element of the initial bands of $J_{AB} \cong 26$ Hz.

This can be understood by taking into account the spread of the initial state on the Bloch sphere. As explained in the main text, dynamical vortices occur when the time-evolved many-body state becomes orthogonal to the initial state and thus also depends on the initial state. Consider an initial state only covering the south pole of the Bloch sphere, which would be the case for perfectly flat bands without residual tunnelling between the A and B sites. Then, dynamical vortices would only occur if the final Floquet Hamiltonian pointed to the equator for some momentum. In our specific system, the Hamiltonian can only cover the equator when it covers the whole Bloch sphere, that is, when the Chern number is non-zero. Hence, dynamical vortices would only appear after quenches into Hamiltonians with finite Chern number.

However, when the initial tunnelling between the A and B sites is finite or the system is not purely prepared in the ground state, then the initial state covers a small area around the south pole of the Bloch sphere. Then, quenches into the vicinity of regions with non-zero Chern number can also give rise to dynamical vortices because the final Hamiltonian does not have to cover the equator, just covering its vicinity for some momenta is sufficient. Thus, the appearance of dynamical vortices in our system is not only sensitive to a change of the topology across the quench, but also to a strong change of the geometry of the eigenstates. The observation of dynamical vortices can therefore serve as a precursor for the topologically non-trivial region.

This example demonstrates that, depending on the initial state, dynamical vortices not only appear when equilibrium phase transitions are crossed during the quench but that they can also appear when an equilibrium phase transition is in the vicinity of the final Hamiltonian. Thus, despite the dependence on the initial state the appearance of dynamical vortices is intimately linked to the existence of equilibrium phase transitions of the underlying final Hamiltonian. This opens up an interesting approach for studying equilibrium phase diagrams with very narrow phase boundaries or in cases in which it is experimentally challenging to reach the ground state.

Analysis of vorticity. To identify the vortices in our phase profiles $\varphi_{k,t}$, we calculated the vorticity for each evolution time t. It is determined as the curl of the gradient of $\varphi_{k,t}$. Usually this quantity is zero, but for phase profiles, which are defined modulo 2π, it obtains finite values at the singular points, that is, at the vortices. It is therefore a convenient measure of the local vorticity. The derivatives are evaluated as finite differences on the natural pixel grid of our images, and the gradient is furthermore symmetrized by averaging of the left and right difference. The position of the vortices is determined to the precision of one pixel and the routine yields a finite vorticity on four neighbouring pixels at a given vortex.

The local nature of this quantity makes it suitable to well resolve the annihilation of the vortex pairs, but it is also susceptible to experimental noise in the phase profiles. Noise can produce many closely spaced vortex–anti-vortex pairs. However, due to our excellent data quality, this happens only far outside the first Brillouin zone (FBZ) and for long evolution times. It is therefore not necessary to apply further spatial filtering.

Figure 3c is obtained by adding up the vorticity images of the shown evolution times t. The resulting trace illustrates the motion of the vortices along their contours. The colour scale bar is truncated to the value of a single vortex to avoid large values from the static vortices, where the signal adds up. The error for a wrong count of the vortex number within the FBZ is therefore very small and certainly smaller than the symbol size in Fig. 3e. For Fig. 4a, we checked the presence of dynamical vortices within the FBZ for each evolution time using the vorticity and by cross-checking with the original phase fields. The static vortices can always be clearly identified and are not counted here.